Muhammad Faizan Shaikh; Park, J.; Park, Y.; Antonino-Daviu, J.; Lee, SB. (2022). Electrical Testing for Detection and Classification of Open Damper Bar and Shorted Field Winding Failures in Wound Field Synchronous Motors. IEEE Transactions on Industry Applications. 58(4):4532-4541. https://doi.org/10.1109/TIA.2022.3167017

Electrical Testing for Detection and Classification of Open Damper Bar and Shorted Field Winding Failures in Wound Field Synchronous Motors

Muhammad Faizan Shaikh, Jongsan Park, Yonghyun Park, Sang Bin Lee, Jose A. Antonino-Daviu

***Abstract* – Broken damper bars and shorted field winding turns degrade the starting and running performance of industrial wound field synchronous motors (WFSMs), and can lead to a forced outage of the motor and driven process. Testing of WFSM rotor windings mainly relies on off-line tests, which cannot be performed frequently and are known to lack reliability. Shorted turns in the field winding can be detected on-line from the airgap flux measurement, but require a sensor to be installed on the stator bore. In this paper, new test methods for detecting and classifying damper and field winding faults based on electrical signals are proposed. The proposed methods can provide remote testing at motor standstill and during the motor starting transient without disassembling the motor. Test results on a 30 kW, salient pole WFSM show that both test methods can provide reliable detection and classification of damper and field winding faults.**

***Index Terms* -- Condition Monitoring, Damper bar, Fault Diagnostics, Field Winding, Motor Testing, Spectral Analysis, Wound Field Synchronous Motor**

I. Introduction

WOUND field synchronous motors (WFSMs) are typically employed in industrial applications that require synchronous speed operation at high efficiency and power factor [1]. The complexity and relatively high cost of the rotor due to the excitation system limits WFSMs to motors with rated power above 5 MW. The reliability of the WFSM driven high output compressors, rolling mills, pumped storage motors, and synchronous condensers is critical to the uninterrupted operation of the industrial process. Recent cases of failures in the excitation circuit, field, and damper (amortisseur) windings in WFSMs have shown that rotor components are important for starting and running performance. It was also shown that these faults can lead to starting failures or forced outages of the motor and the process it drives [2]-[9].

When a WFSM is started, the current induced in the damper bars produces most of the starting torque to accelerate the rotor to synchronous speed, N_{sync}. The damper winding also contributes to stabilizing the rotor speed under load or supply transients during motor operation. The field winding is shorted through a discharge resistor without external dc excitation voltage applied until the rotor reaches 92-95% of N_{sync}. The value of the discharge resistor is typically between 6 to 20 times the field winding resistance [10]. The current induced in the shorted field winding also contributes to the starting torque for accelerating the rotor. DC excitation is applied to the field winding when rotor speed reaches N_{sync} to pull the rotor into synchronism and maintain constant speed operation at N_{sync} [1], [11].

The high thermo-mechanical stress in the damper cage under the starting transient causes cracks to develop in the joint between the bar and end ring. Broken damper bars can therefore spread to adjacent bars that must handle the high starting current and this leads to degraded motor performance. Broken damper bars must be detected to reduce the risk of starting failure or protrusion of the bars into the stator during operation [3]-[7]. The field winding is also exposed to thermal and thermo-mechanical stresses, and centrifugal forces that can degrade and wear the turn insulation leading to shorted turns. Although the motor can continue to operate with shorted field turns, the asymmetry in the magnetic fields between the poles causes once per revolution vibration and reduction in the average magnetic field. The reason that shorted field turns must be monitored is to prevent shorted turns from progressing into ground insulation failure [4]-[9].

Detection of broken damper bars and shorted field winding turns currently relies on visual inspection or off-line tests such as the pole drop test or recurrent surge oscillography [4]-[5], [12]-[15]. However, these tests are time-consuming, require motor disassembly and access to the rotor, which is inconvenient. In addition, both rotor faults present during the operation may not be present at rotor standstill [12]-[14]. Although not verified or accepted in the field, there have been studies on detecting damper and field winding failures [9]-[10], [16]-[22]. In [3], [7], [9]-[10], [16]-[19], the stator current or airgap flux is analyzed during the motor starting transient to detect the faults. However, it was shown that the saliency in the rotor produces identical frequency components as the faults, if the stator current is used. It is shown that the damper and field winding faults can be detected and distinguished with the airgap flux measurement; however, installation of the sensors in the motor is required. In [20]-[21], monitoring of the rotor speed frequency sidebands are

This work was supported by the National Research Foundation of Korea (NRF) grant funded by the Korea government (MSIT) under Grant NRF-2019R1A2C1084104

M. Faizan Shaikh, J. Park, Y. Park, and S. B. Lee are with the Department of Electrical Engineering, Korea University, Seoul, 02841 Korea (e-mail: faizan.shaikh@eecs.korea.ac.kr, jongsan.park@eecs.korea.ac.kr, yonghyun.park@eecs.korea.ac.kr, sangbinlee@korea.ac.kr).

J. Antonino-Daviu is with the Department of Electrical Engineering, Universitat Politècnica de València, Valencia, 46022 Spain (e-mail: joanda @die.upv.es)

proposed for detecting the rotor faults; however, most mechanical defects are known to produce identical components and interfere with fault detection. Monitoring of circulating currents in parallel stator windings are studied in [21]-[22] for detecting shorted field turns, but they require specially wound stators. Stray flux monitoring has also been suggested [23]-[25]; however, it requires installation of additional sensors and cannot be monitored remotely.

On-line monitoring of the airgap flux installed on the stator bore has become common for detecting shorted field turns for synchronous generators [12]-[15], and is being increasingly used for motors. However, most WFSMs are not equipped with airgap flux sensors, which limits its application in the field. Detection of damper and field winding faults is viewed as a difficult task by WFSM manufacturers with challenges to overcome [3], [6]-[7].

Considering the limitations of the methods available for WFSM damper and field winding fault detection, electrical test methods for detecting and classifying the two faults are studied in this paper. Two test methods that can identify the faults at motor standstill and during starting are proposed based on the analysis of the electrical equivalent circuit. It is shown through experimental testing on a custom built 30 kW salient pole WFSM that the proposed methods can provide remote testing without requiring motor disassembly to detect and classify the rotor faults if the measurements are trended over time. The work in this paper is a continuation of the work in [26]-[27] on detecting WFSM rotor faults.

II. Analysis of Open Damper Bar and Shorted Field Winding Turn Failures

In this section, the influence of broken damper bars and shorted field winding turns on the parameters of the per phase electrical equivalent circuit of a salient pole WFSM is analyzed. The concept and principles behind the proposed electrical test methods are explained in III-IV based on the qualitative analysis given in this section. Since testing at motor standstill and during the starting transient is of interest, the electrical equivalent circuits under these conditions are derived based on the *d*-axis and *q*-axis starting equivalent circuits in [28].

The rotor field windings and damper bars of a 4-pole salient pole WFSM are shown in Fig. 1 along with the *d*- and *q*-axes. The *d*-axis and *q*-axis equivalent circuits can be represented as shown in Fig. 2(a)-(b), respectively [28]-[29]. v_{ds}, v_{qs}, i_{ds}, i_{qs} are the *d*- and *q*-axes stator voltages and currents; and R_s and X_{ls} represent the stator resistance and leakage reactance. X_m, R_r, X_{lr}, and s represent the magnetizing reactance, the resistance and leakage reactance of the rotor damper winding, and the rotor slip, respectively. Switch S_{start} is open at motor standstill and closed during the motor starting transient, since the field winding is shorted through a discharge resistor during starting. Hence R_f represents the sum of the field winding and discharge resistances and X_{lf} represents the field winding leakage reactance. Switch S_{short} is closed when a shorted turn is present in the field winding, and open otherwise. The resistance and leakage reactance of the shorted field loop are represented as R_{fs} and X_{lfs}. The decrease in R_f and X_{lf} due to shorted field turns is ignored considering the large number of field turns. Switch S_{sync} is closed at standstill and during acceleration and open when the rotor reaches N_{sync}, since voltage is not induced in the damper. Note that all rotor parameters are referred to the stator.

When the rotor is at standstill, S_{start} is open, S_{sync} is closed and s=1. A broken damper bar results in an increase in all the equivalent lumped rotor damper parameters, R_{rd}, R_{rq}, X_{lrd}, and X_{lrq}. This causes an increase in the input impedance of the equivalent circuits, $Z_{d,eq}$ and $Z_{q,eq}$. Since X_{md} is much larger than X_{mq} in a salient pole rotor, the influence of increase in R_r and X_{lr} is significant in $Z_{d,eq}$, and negligible in in $Z_{q,eq}$. Shorted field winding turns introduce a low impedance shorted loop in the *d*-axis, as can be seen in Figs. 1 and 2(a). Closing S_{short} results in a significant decrease in the *d*-axis equivalent input impedance, $Z_{d,eq}$, and does not influence $Z_{q,eq}$, as can be predicted from Fig. 2.

When the motor is started from standstill, S_{start} and S_{sync} are closed and s decreases towards 0. $Z_{d,eq}$ increases with broken damper bars and decreases with shorted field turns as in the case of standstill, although the degree of change in $Z_{d,eq}$ is

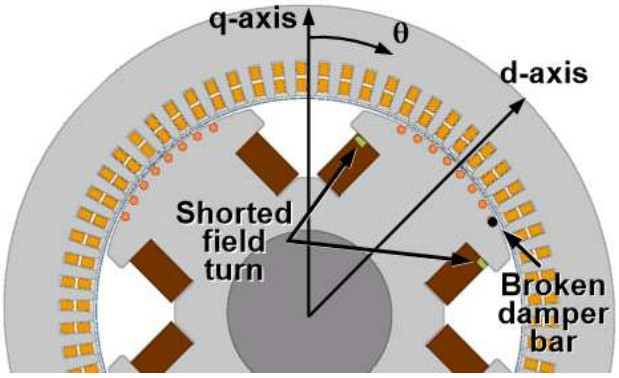

Fig. 1. 4 pole wound field salient pole synchronous motor with broken damper bar and shorted field winding turn. *d*- and *q*-axes shown

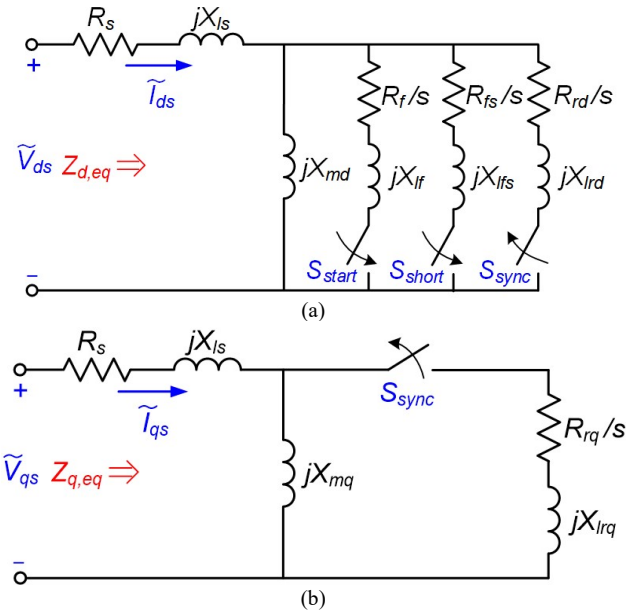

Fig. 2. (a) *d*-axis and (b) *q*-axis electrical equivalent circuit of salient pole WFSM at motor standstill (S_{start}: open, S_{sync}: closed, s=1) and during motor starting (S_{start}: closed, S_{sync}: closed, s=1→0)

different with S_{start} open (s=1). The change in Z_{eq} as a function of electrical position of the field with respect to the rotor q-axis, θ (shown in Fig. 1), is illustrated in Fig. 3 for a salient pole WFSM with healthy and faulty (broken damper bars and shorted field turns) rotors. The equivalent input impedance, Z_{eq}, increases with a broken damper bar and decreases with a shorted field winding turn when the field is aligned to the d-axis, whereas the change is negligible when aligned to the q-axis. This is used as the theoretical basis for detecting and classifying the 2 rotor faults.

When the rotor reaches steady state N_{sync}, there is no voltage induced in the damper winding by the supply frequency f_s as there is no relative motion between the rotor and stator magnetic fields. Thus, the switch S_{sync} in Figs. 2(a)-(b) is open. At N_{sync}, there is also no voltage induced in the field winding supplied with a dc source nor in the shorted field winding loop if a shorted turn exists. Therefore, all the switches S_{start}, S_{short}, and S_{sync} are open and the change in the rotor parameters due to rotor faults does not have any influence on the equivalent input impedance, Z_{eq}. One of the reasons testing at standstill and during the starting transient is considered is because they provide a favorable condition for detecting and classifying the two rotor faults, as can be seen in Fig. 2. With a non-zero slip between N_{sync} and rotor speed, high current is induced in the damper winding and shorted field turn (if it exists) making the change in Z_{eq} easy to observe from terminal electrical measurements. The magnetic saliency effect is increased with open damper bars and reduced with shorted field turns only at motor standstill and during the starting transient, and the WFSM rotor faults are not reflected in Z_{eq} when the motor is operating at N_{sync} in steady state.

III. Off-line Standstill Test for Detection and Classification of WFSM Rotor Failures

It is desirable to test damper and field winding faults under different operating conditions, since the fault present at standstill may not be observable when the motor is operating, and vice versa [12]-[14]. Adding the proposed standstill and starting transient tests to the commercially available tests do not only provide sensitive detection of the faults but can also help in improving the reliability of fault detection. In [18]-[19], detection and classification of damper and field winding faults based on the off-line, single phase rotation test has been proposed. This test has been verified to be very effective for detecting and identifying the type of rotor fault. However, it requires a reduced voltage source (<25% rated voltage) and manual rotation of the rotor in discrete steps [12], [30], which is a non-trivial task for high output motors with heavy rotors. In this work, applying the new type of test presented in [30] for detecting broken rotor bars in induction motors without rotor rotation is proposed for identifying WFSM rotor faults.

The schematic of the proposed off-line standstill test is shown in Fig. 4. The main concept is to use a 3 phase inverter to inject pulsating magnetic fields at multiple angular positions, θ, to extract the equivalent impedance, $Z_{eq}(\theta)$. A 3-phase inverter can be used to inject a low magnitude pulsating field at an arbitrary voltage, V, and frequency, f, given by,

$$\begin{aligned} v_{as}^{*} &= V\cos(\theta).\sin(2\pi f t), \\ v_{bs}^{*} &= V\cos(\theta - 120^{o}).\sin(2\pi f t), \\ v_{cs}^{*} &= V\cos(\theta - 240^{o}).\sin(2\pi f t). \end{aligned} \quad (1)$$

Applying the reference voltages, v^{*}, at θ injects a field that pulsates between θ and θ+180°. The equivalent impedance, for each angular position, $Z_{eq}(\theta)$, can be calculated from the complex space vector of the applied voltage, V_s^{*}, and current measurements, I_s, from

$$Z_{eq}(\theta) = \overrightarrow{V_s^{*}}/\overrightarrow{I_s}, \quad (2)$$

while increasing the value of θ in uniform discrete steps [31]. The magnitude and frequency of the injected field could be set so that torque is not induced in the rotor while providing sufficient resolution in the current (and Z_{eq}) measurement. The power rating of the inverter could be very small compared to the WFSM ratings since impedance measurement does not require high voltage excitation. Therefore, an LV inverter has sufficient monitoring capability for observing the change in z_{eq} between healthy and faulty states. Furthermore, a single, portable LV inverter can be used to test all the WFSMs in the facility when offline. An inverter fed WFSM, on the other hand, can be tested without any additional hardware.

It can be seen that it is possible to obtain the Z_{eq} vs. θ graph shown in Fig. 3 with the proposed method without rotating the rotor. If the trend in the change in the maximum (d-axis) value of the Z_{eq} graph is measured and observed over time, open damper bars and shorted field turns in WFSMs can be detected and classified. Although it is desirable to perform this test at the motor terminal box, it could be run at the MCC for remote monitoring whenever the motor is shut down. The impedance of the cable would be included in the measurements, but can

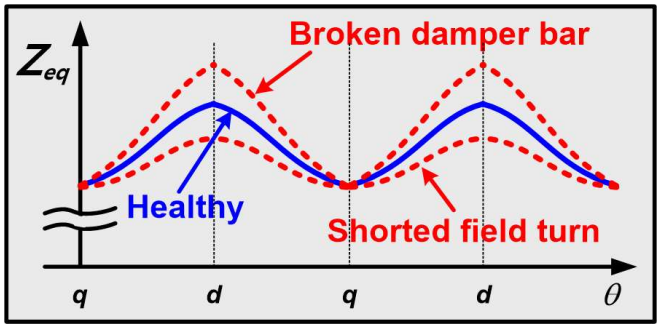

Fig. 3. Equivalent input impedance, Z_{eq}, of salient pole WFSM as a function of rotor electrical position with healthy and faulty rotor (open damper and shorted field turns)

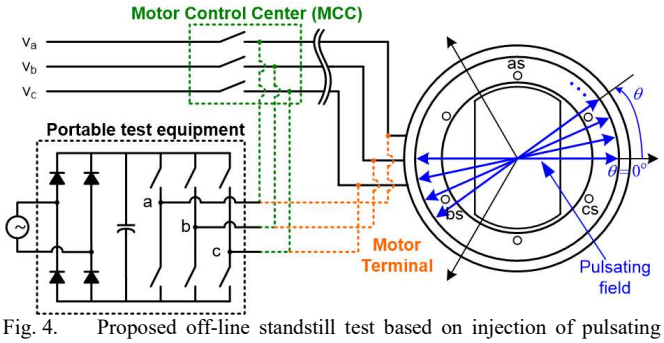

Fig. 4. Proposed off-line standstill test based on injection of pulsating magnetic fields at multiple angular positions, θ

be trended as long as the measurements are consistent. It is also possible to implement the proposed method in SMs fed by inverters. This allows the test to be performed automatically without additional hardware whenever the motor is switched off.

IV. Starting Transient Test for Detection and Classification of WFSM Rotor Failures

The current induced in the damper and shorted field (if any) is high during the starting transient, and therefore, it is also a favorable condition for sensitive detection of the fault. The reliability of fault detection can also be improved since the rotor can be tested under an alternative operating condition of rotor acceleration. When the rotor accelerates from 0 to N_{sync}, the magnitude and frequency of z_{eq} changes with the relative speed between the rotating field and the rotor. From the stator frame of reference, the stator voltage space vector, v_s, can be expressed as,

$$v_s(\omega t) = V_s e^{j\omega_s t}, \tag{3}$$

where V_s and ω_s represent the magnitude and frequency of the stator voltage. The equivalent impedance, z_{eq}, observed from the voltage vector can be expressed as

$$z_{eq}(\omega t) = z_{eq0} - \Delta z_{eq} e^{j2s\omega_s t}, \tag{4}$$

where z_{eq0} and Δz_{eq} represent the average value and magnitude of z_{eq} variation, respectively. When the rotor is at standstill (s=1), z_{eq} changes at a frequency of $2f_s$ since the reluctance due to rotor saliency changes two times per electrical revolution of the rotating field, as can be seen in Fig. 3. When the rotor is rotating at N_{sync} (s=0), z_{eq} is dc as represented in (4). This makes the frequency of change in z_{eq} proportional to twice slip frequency, $2sf_s$, as shown in (4). The equivalent admittance, y_{eq}, can be derived from the inverse of z_{eq} as

$$y_{eq}(\omega t) = y_{eq0} + \Delta y_{eq} e^{-j2s\omega_s t}, \tag{5}$$

where y_{eq0} and Δy_{eq} are the magnitude of the average and varying admittance components, respectively.

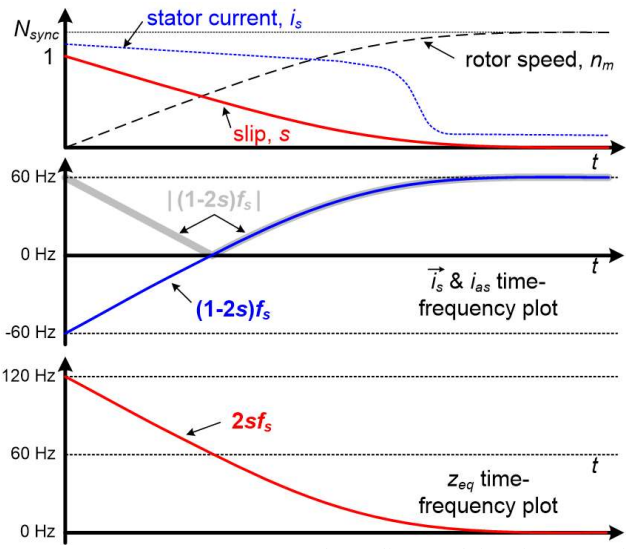

Fig. 5. Stator current, i_s, rotor speed, n_m, slip, s, and time-frequency plot of fault component in i_s space vector, i_{as}, and z_{eq} during the starting transient

The expression for stator current, i_s, can be derived from the product of the voltage vector v_s and y_{eq} shown in (3), (5) as

$$i_s(\omega t) = V_s y_{eq0} e^{j\omega_s t} + V_s \Delta y_{eq} e^{j(1-2s)\omega_s t}. \tag{6}$$

It can be seen that the variation in z_{eq} due to rotor saliency and rotor faults is reflected in the coefficients of the $(1\text{-}2s)f_s$ component of i_s. The saliency can be considered as an asymmetry during WFSM starting transient operation and thus results in $(1\text{-}2s)f_s$ component regardless of the presence of broken bars just like in IMs with axial ducts [32]. Since broken damper bars and shorted field turns result in an increase and decrease in Δz_{eq} (or Δy_{eq}), respectively, they can be observed from the change in the magnitude of the $(1\text{-}2s)f_s$ component of i_s or the $2sf_s$ component of z_{eq}. It can be predicted from Fig. 3 and (3)-(6) that Δz_{eq} and $V_s \Delta y_{eq}$ (in i_s) would increase with a broken damper bar and decrease with a shorted field turn, making identification of the fault from i_s or z_{eq} possible. The instantaneous z_{eq} can be obtained from the space vector of the v_s and i_s measurements as,

$$z_{eq}(\theta) = \vec{v_s}/\vec{\imath_s}. \tag{7}$$

The best way of monitoring and trending the magnitude of specific frequency components of z_{eq} and i_s space vector is to perform Fourier transform. However, the conventional Fourier transform is not suitable since the frequency of the components of interest constantly changes with slip, s, during the starting transient, as shown in Fig. 5. For a 60 Hz input, the $2sf_s$ component of z_{eq} and y_{eq} decreases from 120 to 0 Hz, and the $(1\text{-}2s)f_s$ component of i_s space vector increases from -60 to 60 Hz, as s decreases from 1 to 0. The rotor speed, slip, and the change in the $(1\text{-}2s)f_s$ component of i_s and $2sf_s$ component of z_{eq} during the starting transient are shown in Fig. 5. The influence of the change in z_{eq} due to rotor faults can also be observed from frequency spectrum of the current of a single phase, i_{as}. Since the information on the "direction" of the current space vector rotation is not available in the single phase current, the frequency of the rotor saliency and fault related component is reflected in i_{as} as the absolute value of $(1\text{-}2s)f_s$. Therefore, the rotor fault related components produce a V pattern where it starts at 60 Hz and decreases to 0 and increases back to 60 Hz, as shown in Fig. 5. Note that this can only be achieved if the motor is started directly-online, and not with inverter-fed motor starting.

To observe how the frequency contents of non-stationary signals such as i_s and z_{eq} change with slip during the starting transient, time-frequency transformation is required. Among the different types of transformation techniques available [31], the Short Time Fourier Transformation (STFT) is applied in this work since the computational requirements are relatively low, and STFT has been proven to be effective for detecting motor faults during the starting transient [16]-[19]. An example of the starting current i_{as} waveform and the STFT time-frequency plots of the i_s space vector, z_{eq}, and i_{as} are shown in Fig. 6 for a 30 kW salient pole WFSM with a healthy rotor. The STFT plots show how the frequency contents of the signals change with time. The magnitude of the components is represented as the intensity of the plot at a given instant of

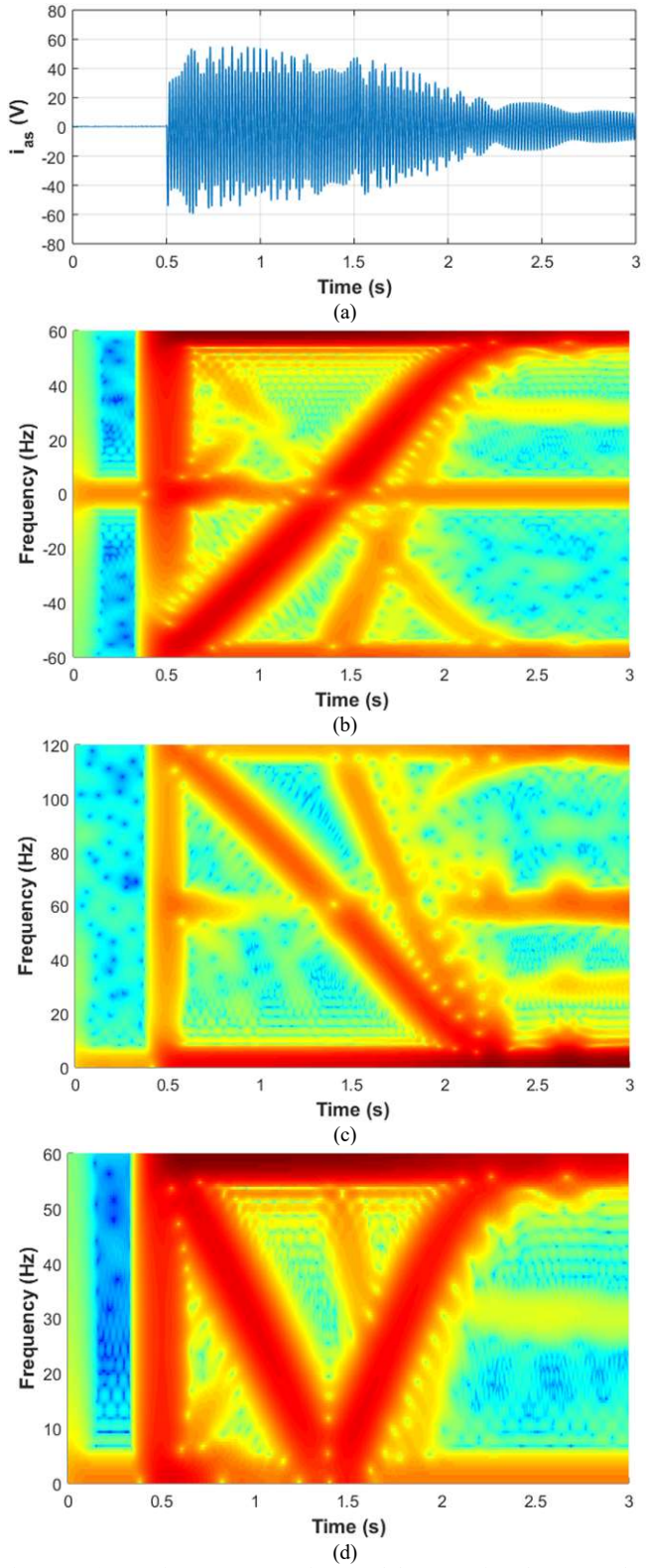

Fig. 6. (a) Starting current waveform, and the STFT time-frequency plots of (b) i_s space vector, (c) z_{eq}, and (d) i_{as} for a 30 kW salient pole WFSM with a healthy rotor

time (x-axis) and frequency (y-axis), where red is highest in magnitude and blue is lowest. The main components in the i_s space vector and i_{as}, which are the 60 Hz component and the $(1\text{-}2s)f_s$ component produced by saliency, as illustrated in Fig. 5, can be clearly observed in Figs. 6(b), (d). The frequency content of z_{eq} is mainly dc, and the $2sf_s$ component produced due to rotor saliency can be also be observed in Fig. 6(c), as slip decreases from 1 to 0.

The magnitude (i.e. intensity) of the above-mentioned slip-dependent components in the current space vector i_s, z_{eq}, and i_{as} increases with a broken damper bar, and decreases with a shorted field winding turn. Therefore, the two rotor faults can be detected and classified if the magnitudes of the components are trended over time. There are many different types of peak tracking algorithms that can be applied. In this work, a simple algorithm which starts at -60 Hz of the i_s space vector STFT plot upon motor starting and tracks the nearest peak value at the next instant of time is sufficient for tracking of the peak of the $(1\text{-}2s)f_s$ component. Similarly, the starting point for the z_{eq} and i_{as} STFT plots could be 120 Hz and 60 Hz, respectively, when the motor is started. Test results of the peak values of the saliency components under damper and field winding failures are shown in V.B.

V. Experimental Study

A. Experimental Setup

The two proposed methods were tested on a 380 V, 30 kW, 4-pole salient pole WFSM prototype shown in Fig. 7. The motor was custom designed and built to resemble the structure of medium-high voltage wound field synchronous motors. Two rotors were built for testing broken damper bars (rotor A) and shorted field turns (rotor B). The rotors have 6 copper damper bars per pole (24 total bars) that are shorted by welding them to two copper laminations on each end. The field winding consists of 144 turns of rectangular magnetic

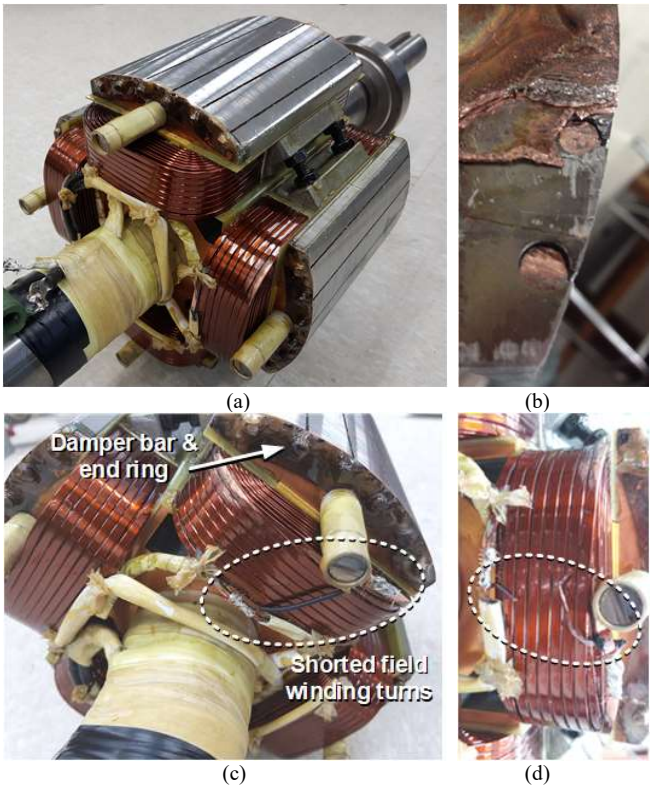

Fig. 7. 380 V, 30 kW, 4 pole salient pole WFSM: (a) rotor; (b) broken damper bars; (c) shorted field winding turns; (d) open circuit of shorted field turn wire during starting transient

wire per pole (576 total turns). 0, 1, and 2 broken damper bar conditions were produced on rotor A by stripping the copper laminations from the bars, as shown in Fig. 7(b). The trailing edge bars are most likely to break due to the uneven distribution of current within the bars of a pole with highest current on the trailing end as reported in [5]-[6]. Therefore, the bars on the trailing edge were broken. Shorted field winding turn condition was produced on rotor B by shorting 7 turns (1.22%) from the same pole using a copper wire, as shown in Fig. 7(c).

The proposed standstill test was performed using a custom built 600 V, 50 A IGBT inverter. 50 V, 50 Hz voltage was applied to produce the pulsating fields in 5° (electrical) intervals from 0° to 360° for obtaining Z_{eq} as a function of θ. The motor was started directly from the main supply after initiating data acquisition to capture the starting data. The voltages and currents of each phase were measured using commercial sensors for both tests. The field winding was open during standstill testing, and shorted through a discharge resistor with a value equal to 10 times of the field winding resistance, which is typical in medium voltage WFSMs.

B. *Experimental Results*

The experimental test results of the proposed off-line standstill test described in III are shown in Fig. 8. The Z_{eq} values are shown as a function of pulsating field angle, θ, for 0, 1, and 2 broken damper bars in rotor A in Fig. 8(a). Z_{eq} vs. θ measured from rotor B with 0 and 7 shorted field turns are shown in Fig. 8(b). It can be seen that the maximum values of Z_{eq} (d-axis values) change with rotor faults whereas the change in the minimum values (q-axis values) is negligible, as predicted in Figs. 2-3. The d-axis value of Z_{eq} increases with the severity of broken damper bars, and decreases with shorted field turns. The results show that the two WFSM rotor faults can be reliably detected and classified with high sensitivity. This is meaningful since the test does not require motor disassembly or manual rotation as in the existing off-line tests. It should be noted that the Z_{eq} measurements for the healthy rotor A and B are different, because there is a slight difference in the airgap.

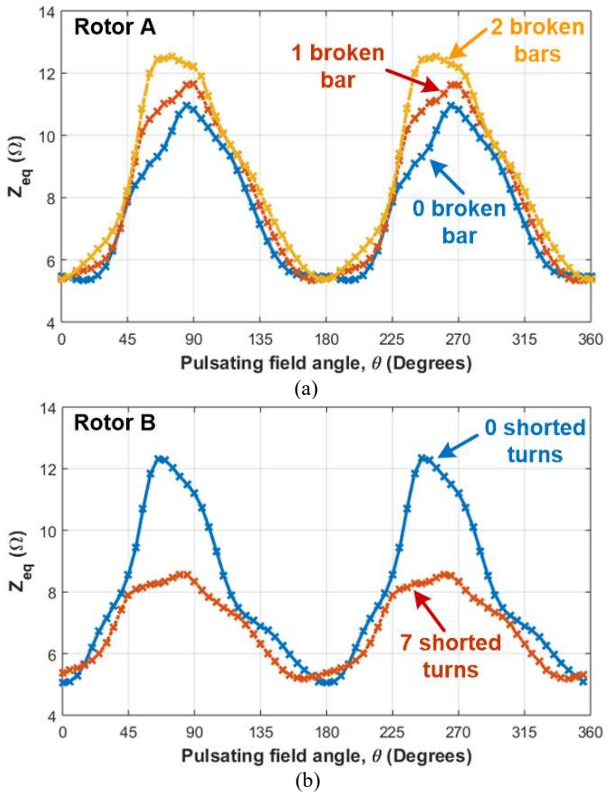

Fig. 8. Experimental results of proposed off-line standstill off-line test: Z_{eq} vs. θ measurement for (a) rotor A under 0, 1, and 2 broken damper bars; (b) rotor B under 0 and 7 shorted field turns

The STFT time-frequency plots of the i_s space vector and z_{eq} under the starting transient are shown in 3-dimensional view in Figs. 9-10, respectively. The STFT plots under 2 broken damper bars (rotor A) and 7 shorted field winding turns (rotor B) are shown in (a) and (b) of Figs. 9-10, respectively. It can be seen that the pattern under rotor faults are identical to that of the healthy case shown in Figs. 6(b)-(c). To observe the change in the $(1\text{-}2s)f_s$ component in the i_s space vector and $2sf_s$ component in z_{eq}, the peak values have been tracked using the simple algorithm described in IV and highlighted in black dotted lines. For i_s shown in Fig. 9, tracking of the peak value was started at t = 0 s, f = -60 Hz, and the neighboring peaks within the range of ±2 Hz from the present frequency were tracked at the next instant of time. For z_{eq} in Fig. 10, the starting point was t = 0 s, f = 120 Hz, as shown in Fig. 10.

The peak values of the $(1\text{-}2s)f_s$ component in the i_s space vector (Fig. 9) during the starting transient with 0, 1, and 2 broken damper bars (rotor A) are shown in Fig. 11(a), and the peak values with 0 and 7 field winding turns shorted (rotor B) are shown in Fig. 11(b). The peak values of the $2sf_s$ components in z_{eq} (Fig. 10), are shown in Figs. 12(a)-(b) for

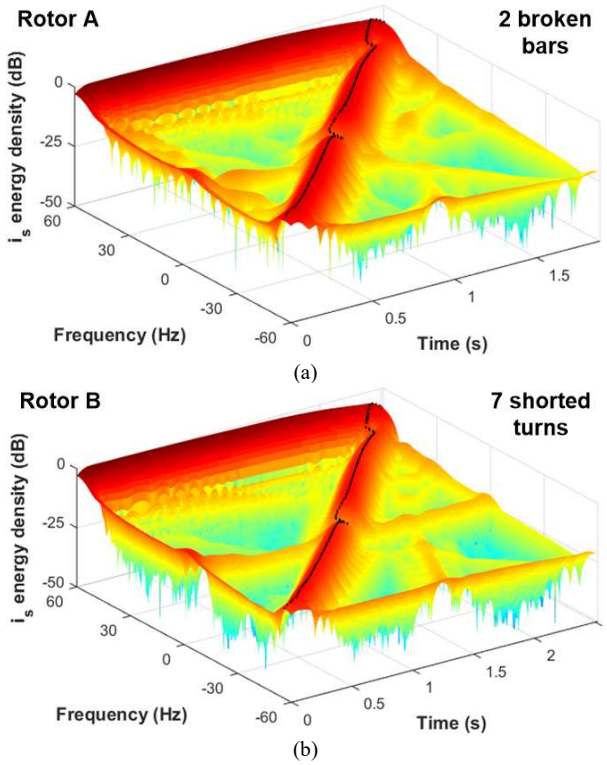

Fig. 9. 3D STFT time-frequency plots of i_s space vector under (a) 2 of 24 broken damper bars and (b) 7 of 576 shorted turns in 30 kW salient pole WFSM with tracking of peak saliency component $(1\text{-}2s)f_s$ shown

broken damper bars and shorted field winding turns, respectively. Since the duration of starting time can change depending on the load and with rotor faults, time has been normalized to the starting period of the healthy rotor for comparing the magnitudes under similar rotor slip conditions. The peak values have also been normalized to the average peak values of the healthy case.

It can be seen in Figs. 11-12 that the saliency related peaks in i_s and z_{eq} increase with the severity of broken damper bars, and decrease with shorted field winding turns, as predicted in IV. This is due to the change in z_{eq} with damper and field winding faults, where broken damper bars increase the effective saliency and shorted field turns decrease the effective saliency, as described in II-IV. The change in the peaks is significant considering the small percentage of broken damper bars or shorted field turns. This allows sensitive detection compared to existing off-line (pole drop test) or on-line (flux probe) tests that rely on detecting the small asymmetry caused by these faults.

Since the i_s space vector requires the starting current of all 3 phases, the proposed method was applied to the STFT plot of single phase current i_{as} as shown in Fig. 6(d) to observe if it is possible to detect the fault with a single-phase current. The results of the peak $(1\text{-}2s)f_s$ components in i_{as} are plotted in Fig. 13(a)-(b) for damper and field winding faults. The peak components were tracked starting at $t = 0$ *s*, 60 Hz in the same way as i_s space vector and z_{eq} under 0 and 2 broken damper bars (rotor A), and 0 and 7 shorted field turns (rotor B). It can be seen that the peak extracted from i_{as} exhibits a similar pattern as that of the i_s space vector shown in Fig. 11 with

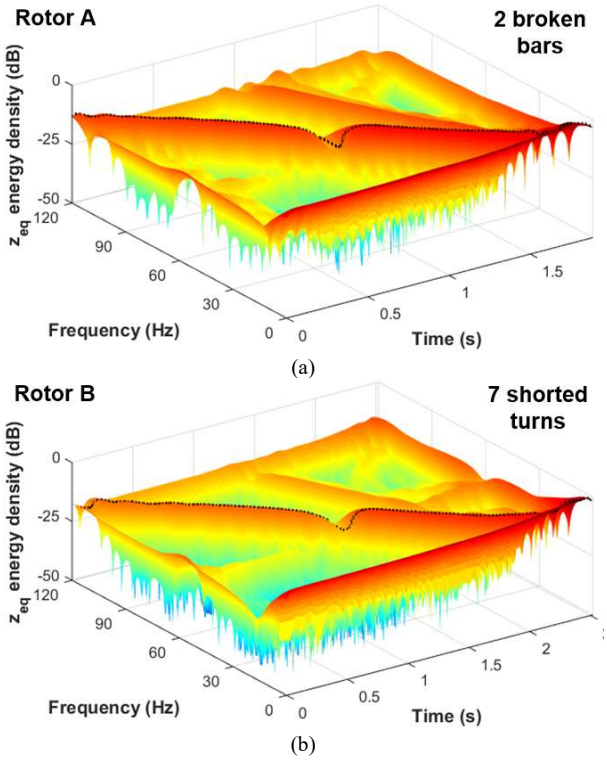

Fig. 10. 3D STFT time-frequency plots of z_{eq} under (a) 2 of 24 broken damper bars and (b) 7 of 576 shorted turns in 30 kW salient pole WFSM with tracking of peak saliency component $2sf_s$ shown

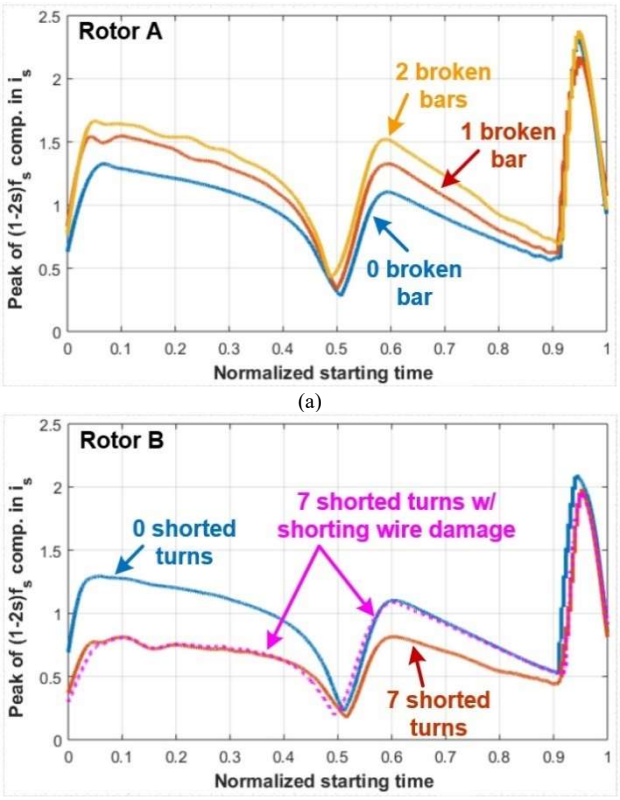

Fig. 11. Peak of $(1\text{-}2s)f_s$ component in STFT time-frequency plot of i_s space vector under (a) 2 of 24 broken damper bars and (b) 7 of 576 shorted turns in 30 kW salient pole WFSM

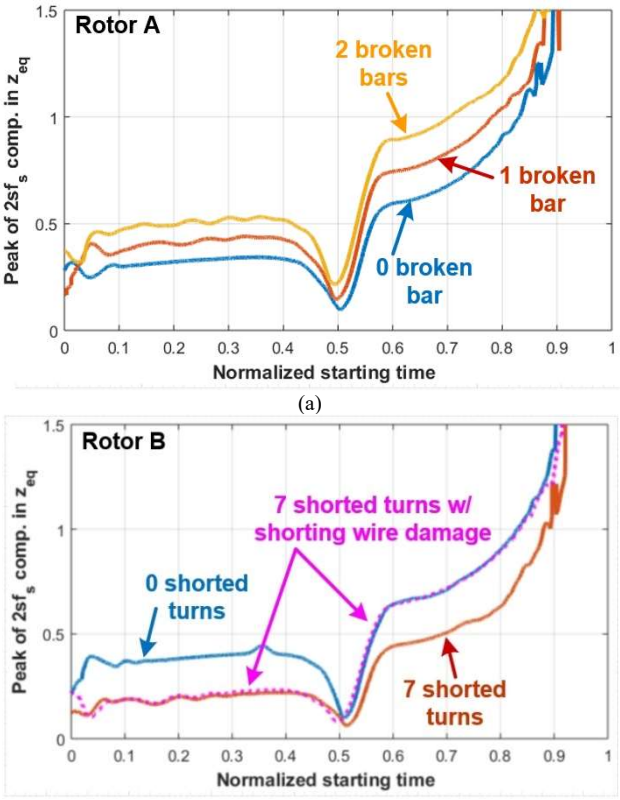

Fig. 12. Peak of $2sf_s$ component in STFT time-frequency plot of z_{eq} under (a) 2 of 24 broken damper bars and (b) 7 of 576 shorted turns in 30 kW salient pole WFSM

lower sensitivity. This can be attributed to the fact that the

negative sequence component cannot be separated with single phase current, and that there is overlap between the 60 Hz and the absolute value of $(1\text{-}2s)f_s$ component in the beginning of the starting transient, as can be seen in Figs. 6(b) and (d). The average of the peaks for the healthy case, to which the fault indictor is normalized to, is also higher, making the values different. Comparison of Figs. 11 and 13 show that it is possible to detect and classify the two faults with a single-phase current although there is a reduction in sensitivity.

The starting test was performed twice with shorted field turns, and the peak saliency components were always lower than that of the healthy rotor for the first test, as shown in Figs. 11(b), 12(b), and 13(b). However, during the second test, smoke was observed, and the peak values were similar to that of the faulty case for the first half, while for the second half of the starting period, they became similar to the healthy case, as shown by dotted lines in Fig. 11(b), 12(b), and 13(b). When the field winding was visually inspected after the test, the wire used for shorting the 7 field winding turns was found to be open-circuited due to severe overheating, as shown in Fig. 7(d). Although this was not intended, the results show that intermittent short circuits during the starting transient can be detected. This is an important advantage since intermittent contact is known to produce false indications in both standstill and on-line testing. The test results in Figs. 11-13 clearly show that the STFT plot of the i_s space vector, z_{eq}, or i_{as} can be used for sensitive and reliable detection and classification of damper and field winding failures in WFSMs.

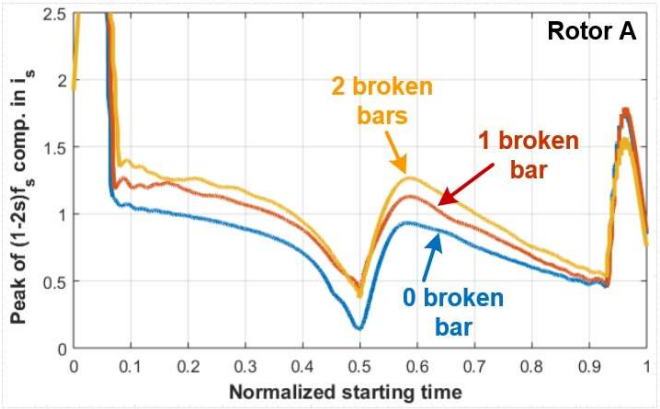

(a)

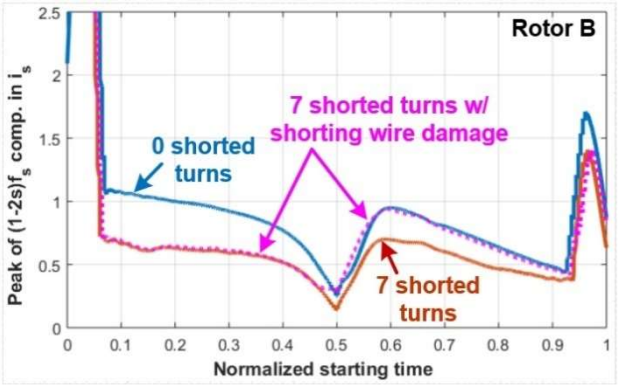

(b)

Fig. 13. Peak of $(1\text{-}2s)f_s$ component in STFT time-frequency plot of i_{as} under (a) 2 of 24 broken damper bars and (b) 7 of 576 shorted turns in 30 kW salient pole WFSM

VI. Conclusion

Electrical test methods capable of remote detection and classification of damper and field winding faults in WFSMs without motor disassembly have been proposed in this paper. The first test is an off-line standstill test that does not require motor disassembly or manual rotor rotation, and the second test is based on time-frequency analysis of electrical quantities measured during the starting transient. Standstill and starting transient conditions provide a favorable condition for detection of the rotor faults since the current induced in the damper bars and shorted field turns (if any) is high. The faults are not observable from terminal electrical measurements during steady state operation since there is no current induced. Experimental testing on a 30 kW WFSM was performed to verify the claims made on the advantages of the proposed test methods. The proposed tests are expected to provide an alternative option for remote detection and classification of WFSM rotor faults in the field with improved sensitivity and reliability over existing tests.

VII. References

[1] G. Oscarson, J. Imbertson, B. Imbertson, S. Moll, "The abc's of synchronous motors," *WEG group*, 2012.

[2] T. Figel, J. Bothwell, W. Moore, "Preventive maintenance and overhaul experience for rotating brushless exciters and other excitation systems, *Proc. of EPRI utility generator predictive maintenance and refurbishment conference*, 1998.

[3] H.C. Karmaker, "Broken damper bar detection studies using flux probe measurements and time-stepping finite element analysis for salient-pole synchronous machines," *Proc. IEEE SDEMPED*, pp. 193-197, 2003.

[4] S. Orchuk, "Synchronous motors: methods for quantifying rotor condition," *IEEE Ind. Appl. Mag.*, vol. 25, no. 6, pp. 44-54, Nov./Dec. 2019.

[5] I. Kerszenbaum, *Inspection of large synchronous machines: checklists, failure identification, and troubleshooting*, Wiley-IEEE Press, Apr. 1996.

[6] S.K. Sahoo, P. Rodriguez, M. Sulowicz, "Comparative investigation of fault indicators for synchronous machine failures," *Proc. of ICEM*, pp. 1503-1509, 2014.

[7] P. Rodriguez, "Large SM condition monitoring challenges and pitfalls," *Keynote Address, IEEE SDEMPED*, Aug. 2017.

[8] T. D. Batzel, D. C. Swanson, J. F. Defenbaugh, "Predictive diagnostics for the main field winding and rotating rectifier assembly in the brushless synchronous generator," *Proc. of IEEE SDEMPED*, pp. 349-354, 2003.

[9] P.J. Berry, E.S. Hamdi, "An investigation into damper winding failure in a large synchronous motor," *Proc. of Int'l Univ. Power Eng. Conf.*, pp. 1-4, 2015.

[10] J. Yun *et al*., "Comprehensive monitoring of field winding short circuits for salient pole synchronous motors," *IEEE Trans. Energy Convers.*, vol. 34, no. 3, pp. 1686-1694, Sept. 2019.

[11] R. C. Schaefer, "Excitation control of the synchronous motor," *IEEE Trans. Ind. Appl.*, vol. 35, no. 3, pp. 694-702, May-June 1999.

[12] G.C. Stone, I. Culbert, E.A. Boulter, H. Dhirani, *Electrical insulation for rotating machines – design, evaluation, aging, testing, and repair*, IEEE Press Series on Power Engineering, John Wiley and Sons, 2014.

[13] M. Sasic, G.C. Stone, J. Stein, C. Stinson, "Detecting Turn Shorts in Rotor Windings: A New Test Using Magnetic Flux Monitoring," *IEEE Ind. Appl. Mag.*, vol. 19, no. 2, pp. 63-69, Mar./Apr. 2013.

[14] D.R. Albright, "Interturn Short-Circuit Detector for Turbine-Generator Rotor Windings," *IEEE Trans. on Power App. Syst*, vol. PAS-90, no. 2, pp. 478-483, Mar. 1971.

[15] Field testing of continuous flux monitoring for hydrogenerators: feasibility study, EPRI and New York Power Authority, 2004.

[16] J.A. Antonino-Daviu, *et al*, "Toward Condition Monitoring of Damper Windings in Synchronous Motors via EMD Analysis," *IEEE Trans. Energy Convers.*, vol. 27, no. 2, pp. 432-439, June 2012.

[17] J. Antonino-Daviu, V. Climente-Alarcon, A. Q. López and S. Hornsey, "Reporting false indications of startup analysis when diagnosing damper damages in synchronous motors," *Proc. of IEEE INDIN,* pp. 434-438, 2016.
[18] J. Yun et al., "Airgap search coil-based detection of damper bar failures in salient pole synchronous motors," *IEEE Trans. Ind. Appl.*, vol. 55, no. 4, pp. 3640-3648, July/Aug. 2019.
[19] Y. Park, S.B. Lee, J. Yun, M. Sasic, and G.C. Stone, "Detection and Classification of Damper Bar and Field Winding Faults in Salient Pole Synchronous Motors," *Proc. of IEEE ECCE*, pp. 4491-4498, Sept. 2019.
[20] P. Neti, A.B. Dehkordi, A.M. Gole, "A new robust method to detect rotor faults in salient-pole synchronous machines using structural asymmetries," *Proc. of IEEE IAS,* pp.1-8, Oct. 2008.
[21] J. Sottile, F.C. Trutt, A.W. Leedy, "Condition Monitoring of Brushless Three-Phase Synchronous Generators With Stator Winding or Rotor Circuit Deterioration," *IEEE Trans. Ind. Appl.*, vol. 42, no. 5, pp. 1209-1215, Sept./Oct. 2006.
[22] J.W. Wood, R.T. Hindmarch, "Rotor winding short detection," *IEE Proc. Pt. B – Elect. Power Appl.*, vol. 133, no. 3, pp. 181-189, May 1986.
[23] O. Chadebec *et al.*, "Rotor Fault Detection of Electrical Machines by Low Frequency Magnetic Leakage Field Analysis", *Proc. 5th IEEE Int. SDEMPED*, 2005 pp. 1–6.
[24] M. Cuevas *et al.*, "Noninvasive Detection of Winding Short-Circuit Faults in Salient Pole Synchronous Machine With Squirrel-Cage Damper," *IEEE Trans. Ind. Appl.*, vol. 54, no. 6, pp. 5988-5997, Nov./Dec. 2018.
[25] M. F. Shaikh, J. Park and S. B. Lee, "A Non-Intrusive Leakage Flux based Method for Detecting Rotor Faults in the Starting Transient of Salient Pole Synchronous Motors," *IEEE Trans. Energy Convers.*, early access. doi: 10.1109/TEC.2020.3021207.
[26] J. Antonino-Daviu et al., "Electrical monitoring of damper bar condition in salient pole synchronous motors without motor disassembly," *Proc. of IEEE SDEMPED*, pp. 62-68, 2019.
[27] M. F. Shaikh, J. Park, Y. Park, S.B. Lee, "Electrical Testing for Detection and Classification of Open Damper Bar and Shorted Field Winding Failures in Wound Field Synchronous Motors," *Proc. of SDEMPED*, pp. 72-78, 2021.
[28] H.A. Toliyat, G.B. Kliman, *Handbook of Electric Motors*, Marcel Dekker, 2004.
[29] P.C. Krause, O. Wasynczuk, S.D. Sudhoff, *Analysis of Electric Machinery and Drive Systems*, Wiley-IEEE Press, 2002.
[30] B. Kim, K. Lee, J. Yang, S. B. Lee, E. J. Wiedenbrug, and M. R. Shah, "Automated Detection of Rotor Faults for Inverter-Fed Induction Machines Under Standstill Conditions," *IEEE Trans. Ind. Appl.*, vol. 47, no. 1, pp. 55-64, Jan.-Feb. 2011.
[31] L. Cohen, *Time-Frequency Analysis*. A.V. Oppenheim, Ed. Prentice Hall Signal Processing Series, New Jersey, 1995.
[32] S. Lee *et al.*, "Evaluation of the influence of rotor axial air ducts on condition monitoring of induction motors," *IEEE Trans. Ind. Appl.*, vol. 49, no. 5, pp. 2024-2033, Sept.-Oct. 2013.

VIII. BIOGRAPHIES

Muhammad Faizan Shaikh received his B.E. degree in electrical engineering from NED University of Engineering and Technology, Karachi, Pakistan, in 2016 and his M.E. degree in electrical engineering from Korea University Seoul, Korea. He is currently pursuing his PhD degree in electrical engineering, also at Korea University, Seoul, Korea.

He was an intern in RF optimization Dept. at Ericsson, Pakistan, in 2016, a Maintenance Trainee Engineer in National Refinery Limited, Pakistan in 2016. He worked as an Operations Trainee Engineer at Chongxin Coal Fired Power Plant, Gansu Province, China from 2016 to 2017 and at Port Qasim Coal Fired Power Plant, Karachi, Pakistan from 2017 to 2018 under Power China Gansu Energy Investment Co., Ltd. His research interests are condition monitoring and analysis of electrical machinery.

Jongsan Park received his B.E. degree in electrical engineering from Korea University, Seoul, Korea, in 2019. He is pursuing master's degree in electrical engineering at Korea University, Seoul, Korea. His research interests are in electric machinery and condition monitoring.

Yonghyun Park (S'14) received his B.E. degree in electrical engineering from Korea University, Seoul, Korea, in 2014. He is currently pursuing Ph.D. degree in electrical engineering at Korea University, Seoul, Korea. He was a Summer intern at Polytechnic University of Valencia, Valencia, Spain in 2015, and a Winter intern at University of Oviedo, Gijon, Spain in 2016. His research interests are in condition monitoring and analysis of electric machinery.

Sang Bin Lee (S'95-M'01-SM'07-F'17) received his B.E. and M.E. degrees from Korea University, Seoul, Korea in 1995 and 1997, respectively, and his Ph.D. degree from Georgia Institute of Technology, Atlanta, GA in 2001, all in electrical engineering.

From 2001 to 2004, he was with General Electric Global Research Center (GRC), Schenectady, NY, as a Research Scientist. From 2010 to 2011, he was with the Austrian Institute of Technology, Vienna, Austria, as a Visiting Scientist. From 2017 to 2018, he was a Consultant at Qualitrol - Iris Power Engineering, Toronto, and a Visiting Researcher at University of Waterloo, ON, Canada. Since 2004, he has been a Professor of electrical engineering at Korea University, Seoul, Korea. His current research interests are in monitoring and diagnostics of electric machines and drives.

Dr. Lee was the recipient of 2017 IEEE SDEMPED Diagnostics Achievement Award, and received fifteen IEEE society- and committee-level Prize Paper Awards. He served as a 2014-2016 Distinguished/ Prominent Lecturer for IEEE IAS, and as an Associate Editor for the IEEE TRANSACTIONS ON INDUSTRY APPLICATIONS for the IEEE IAS Electric Machines Committee.

Jose A. Antonino-Daviu (S'04-M'08-SM'12) received his M.S. and Ph. D. degrees in Electrical Engineering, both from the Universitat Politècnica de València, in 2000 and 2006, respectively. He also received his BS. in Business Administration from Universitat de Valencia in 2012.

Currently, he is an Associate Professor in the Instituto Tecnológico de la Energía Universitat, Politècnica de València, where he develops his docent and research work. He has been an invited professor in Helsinki University of Technology, Helsinki, Finland in 2005 and 2007, Michigan State University, East Lansing, Michigan, USA in 2010, Korea University, Seoul, Korea in 2014, and Université Claude Bernard Lyon, Lyon, France in 2015. He has over 100 publications in international journals, conferences, and books.

He serves as an Associate Editor of the IEEE Transactions on Industrial Informatics and has been a Guest Editor for the IEEE Transactions on Industrial Electronics. He was a General Co-Chair of IEEE SDEMPED 2013.